analytical chemistry

pubs.acs.org/ac Article

# Photoelectrochemical Assay Based on $SnO_2$/BiOBr p−n Heterojunction for Ultrasensitive DNA Detection

Dan Long, Yupeng Tu, Yaqin Chai,* and Ruo Yuan*

Cite This: *Anal. Chem.* 2021, 93, 12995−13000 Read Online

ACCESS | Metrics & More | Article Recommendations | Supporting Information

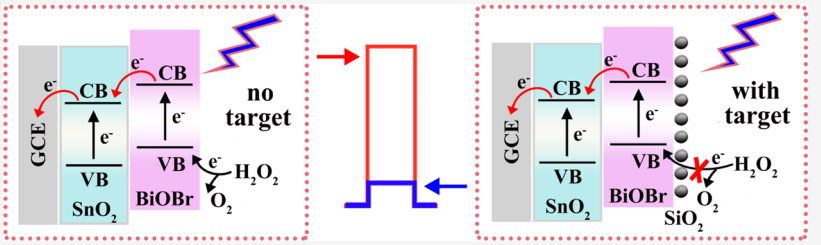


**ABSTRACT:** Herein, a photoelectrochemical (PEC) assay was designed for a highly sensitive DNA determination relying upon the $SnO_2$/BiOBr p−n heterojunction as a photoactive material and $SiO_2$ as a signal quencher. Compared with most traditional heterojunctions, the $SnO_2$/BiOBr p−n heterostructure not only lessened the recombination of the photogenerated electron−hole pairs but also promoted the light-harvesting in the ultraviolet−visible (UV−vis) region, leading to further enhanced photoelectric conversion efficiency and photocurrent, which demonstrated 12.1-fold and 6.4-fold increments versus those of pure $SnO_2$ and BiOBr, respectively. Additionally, the limited quantity of target DNA (a fragment of p53 gene) could be transformed into abundant output DNA−$SiO_2$ by employing the Nt·BstNBI enzyme-assisted signal amplification procedure, leading to a highly improved detection sensitivity of the biosensor. Then, output DNA−$SiO_2$ hybridized with the capture DNA anchored on the modified electrode surface, remarkably diminishing the PEC signal and thus achieving sensitive DNA determination. The elaborated PEC biosensor demonstrated outstanding performance within the linear range between 0.5 fM and 5 nM and a low limit of detection down to 0.18 fM, paving a new way for fabricating heterojunction with exceptional photoactive performance and demonstrating the enormous potential for detecting multitudinous biomarkers in bioanalysis and clinical therapy.



## INTRODUCTION

Photoelectrochemical (PEC) analysis, as a thriving analytical technique, not only has the merits of simple operation and low cost but also possesses the advantages of low background noise and high sensitivity owing to the total separation of excitation light source and the detection signal, gathering tremendous attention in recent years.[1−6] As is well known, the photoelectric conversion efficiency of the photoactive material makes great difference on the performance of PEC biosensors.[7,8] Reducing the electron−hole pair recombination probability and enhancing the light absorption in the ultraviolet−visible (UV−vis) region are effective ways to promote the photoelectric conversion efficiency of photoelectric material.[9] Unfortunately, single photoelectric materials usually have the disadvantage of low photoelectric conversion efficiency, which limits their practical applications.[10,11] In recent years, the construction of heterojunctions is considered to be a feasible and effective way to facilitate the electron−hole separation and restrain the recombination of electron−hole of optoelectronic materials.[12−15] For instance, Xiong's group synthesized a ZnO/$CeO_2$ Z-scheme heterojunction for photodegradating rhodamine B.[16] Lately, Niu's group constructed a $MoS_2$/ZnO p−n heterostructure for propyl gallate determination.[17] Although these heterojunctions have acquired bright achievements in restraining the recombination of electron−hole pairs and promoting charge separation, they are still limited in enhancing the absorption in the UV−vis light region. Therefore, presenting an elaborate heterostructure to conquer the shortcoming is desired.

$SnO_2$, an n-type semiconductor, has been extensively employed in solar cells,[18,19] $CO_2$ electroreduction,[20,21] and photocatalysis[22,23] by virtue of the desirable stability, nontoxicity, and prominent photoelectric properties.[24] Unfortunately, similar to $TiO_2$, it suffers from a large band gap (~3.6 eV)[22,25] as well as fast photogenerated electron−hole pairs recombination, hindering its direct application in PEC biosensing. Unique laminar structure endows BiOBr with extraordinary photocatalytic activity.[26,27] In addition, it takes on satisfying chemical stability and a suitable band gap (~2.6

Received: June 30, 2021
Published: September 15, 2021




https://doi.org/10.1021/acs.analchem.1c02745
*Anal. Chem.* 2021, 93, 12995−13000

Scheme 1. Schematic Illustration of this PEC Assay for DNA Detection Based on the $SnO_2$/BiOBr Heterostructure[a]

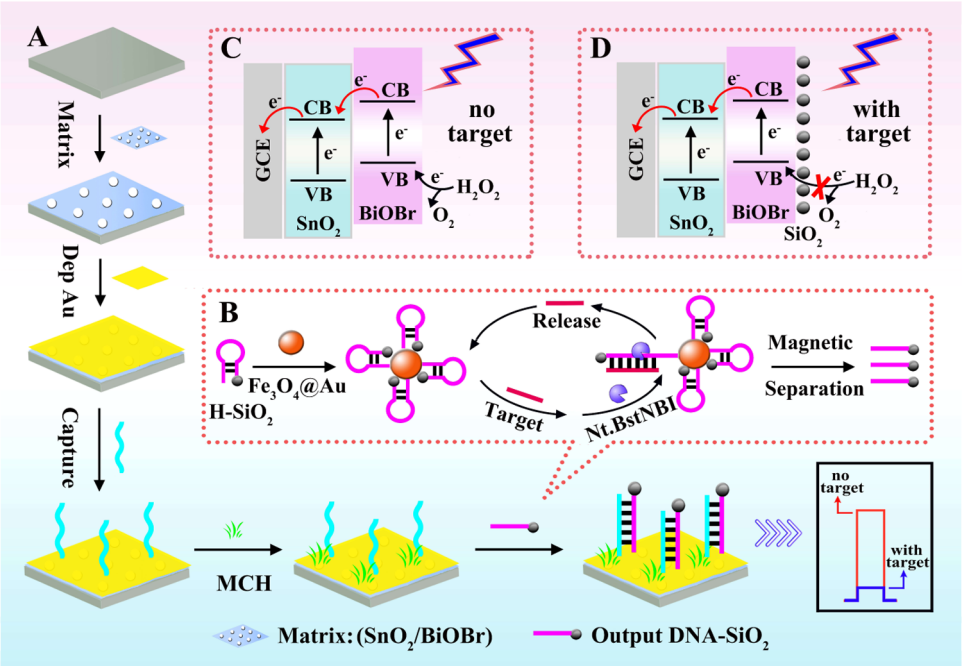


[a](A) Biosensor assembly procedure. (B) Enzyme-assisted signal amplification process. (C, D) Photocurrent generation mechanism.

eV).[28,29] Most importantly, it has been proved that the $SnO_2$/BiOBr heterostructure with the property of stable and low cost demonstrated fascinating performance in photocatalysis.[24,30] Inspired by these findings, an exquisite "signal off" PEC biosensor was developed by employing $SnO_2$/BiOBr heterostructure as the photoactive matrix for the sensitive detection of target DNA. Besides, the enzyme-assisted signal amplification process versus the high-efficiency signal quencher $SiO_2$ were coupled in this strategy for improving the sensitivity of this PEC biosensor.

In this protocol, a PEC biosensor employing a $SnO_2$/BiOBr p−n heterojunction as a photoactive material quenched by $SiO_2$ was fabricated for ultrasensitive target DNA detection. As depicted in Scheme 1, the $SnO_2$/BiOBr complex coated on the electrode surface served as a signal indicator to achieve an intense initial photocurrent signal. Next, the Au nanoparticle (Au NP) layer was obtained by deposition for immobilizing the capture DNA. Subsequently, the capture DNA hybridized with plenty of output DNA−$SiO_2$ attained by the enzyme-assisted signal amplification procedure, causing $SiO_2$ approach to the interface of the biosensor and resulting in significantly reduced photocurrent response as $SiO_2$ has a huge steric-hindrance effect. Consequently, the developed PEC biosensor could complete quantitative DNA detection with high sensitivity and great accuracy. This PEC strategy not only offered a bright path for fabricating other heterostructures with prominent PEC property but also illustrated a huge potential for detecting other analytes.

## EXPERIMENTAL SECTION

**Synthesis of $SnO_2$/BiOBr, $Fe_3O_4$@Au, and Hairpin DNA−$SiO_2$ Conjugate.** $SnO_2$/BiOBr was synthesized by a one-step hydrothermal method according to the reported literature[30] with some modification. Briefly, stannic chloride hydrated ($SnCl_4·5H_2O$, 1.5 mM) was added into a mixture containing 5 mL of ethanol and 5 mL of NaOH (6 mM) under stirring for 0.5 h to form $Sn(OH)_4$ solution. Meanwhile, 2.4 mM potassium bromide (KBr) and bismuth nitrate pentahydrate ($Bi(NO_3)_3·5H_2O$) were added to the mixture including 14 mL of ethylene glycol and 6 mL of $H_2O$ for 0.5 h stirring. Thereafter, the above two solutions were mixed with ultrasonication for another 0.5 h. After that, the attained mixture solution was transferred into a 50 mL Teflon-lined autoclave and kept for 10 h at 110 °C. Then, the obtained white precipitate was carefully washed with water and ethanol for several times and dried at 60 °C overnight. $Fe_3O_4$@Au was prepared according to the previous method.[31] Hairpin DNA−$SiO_2$ conjugate (H-$SiO_2$) was obtained by stirring the mixture of 5 μL of glutaraldehyde, 400 μL of hairpin DNA (2.5 μM), and 400 μL of amino-modified $SiO_2$ nanoparticles ($SiO_2$-$NH_2$ NPs) at room temperature for 1 h. The preparation of $SiO_2$-$NH_2$ NPs is available in the Supporting Information, which was attained according to the reported work[32] with a little modification.

**Enzyme-Assisted Signal Amplification Procedure.** Briefly, 200 μL of H-$SiO_2$ and $Fe_3O_4$@Au were mixed with stirring at 4 °C for 12 h, making $Fe_3O_4$@Au covalently connect with hairpin DNA through Au−S bonds. Then, the obtained mixture was centrifuged and dispersed in 200 μL of 0.1 M phosphate buffer solution (pH 7.0) to remove unreacted reagents. Subsequently, the above mixture was subjected to 100 μL of target DNA at 37 °C with 0.5 h incubation to open the hairpin DNA. After that, for accomplishing the enzyme-assisted signal amplification process, 10× NE buffer (10 μL) and Nt·BstNBI enzyme (20 U) were added to the above mixture with 55 °C incubation for 1 h. Next, to deactivate the enzyme, the mixture was treated for 20 min at 80 °C. Lastly, plenty of output DNA−$SiO_2$ was acquired after magnetic separation.

**Fabrication of the Sensing Platform.** The bare glassy carbon electrode (GCE) was pretreated based on the previous method to achieve a mirror-like surface.[33] Then, 10 μL of


https://doi.org/10.1021/acs.analchem.1c02745
Anal. Chem. 2021, 93, 12995−13000

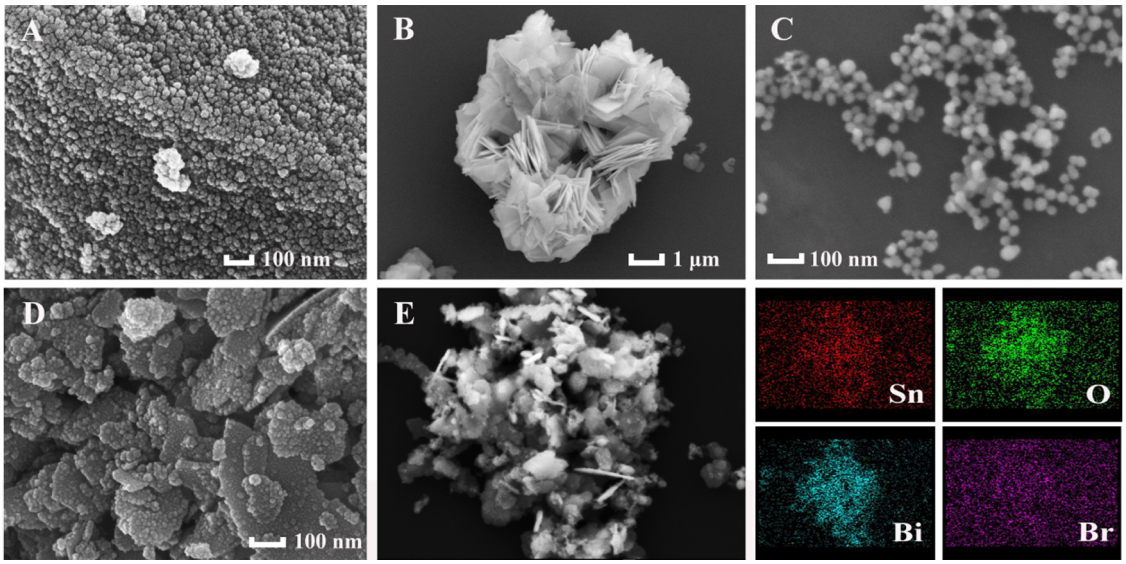


**Figure 1.** SEM images of (A) $SnO_2$, (B) BiOBr, (C) $SiO_2$ NPs, and (D) $SnO_2$/BiOBr complex. (E) SEM image and corresponding elemental mapping images of $SnO_2$/BiOBr complex.

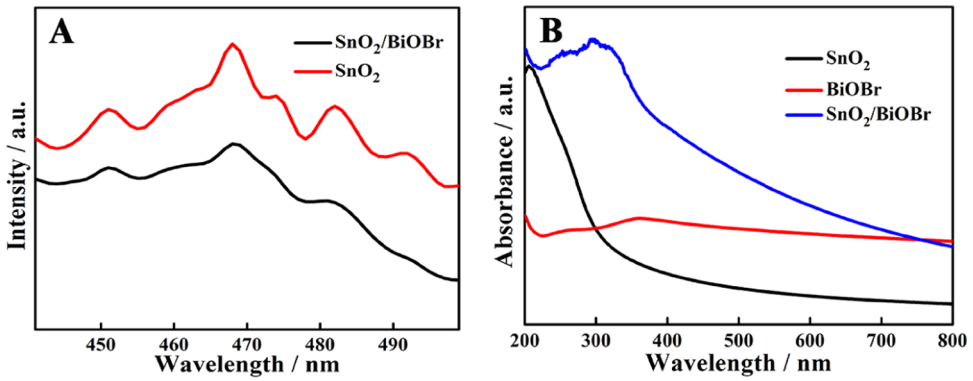


**Figure 2.** (A) PL spectra of $SnO_2$ and $SnO_2$/BiOBr. (B) UV−vis absorption spectroscopy of $SnO_2$, BiOBr, and $SnO_2$/BiOBr.

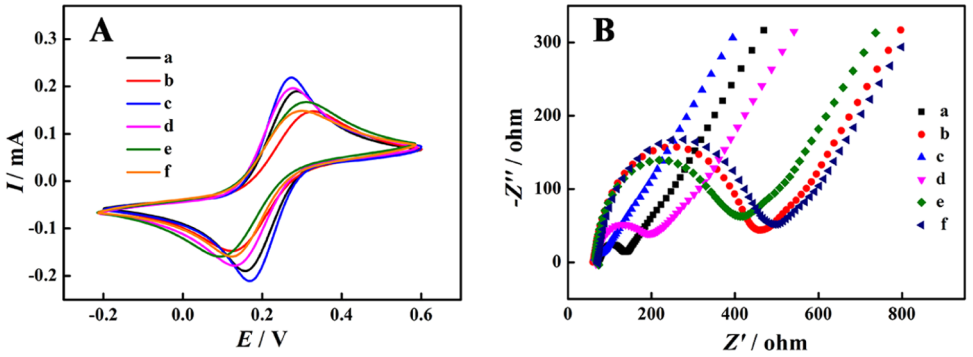


**Figure 3.** Electrochemical characterizations of (A) CV and (B) EIS response: (a) bare GCE, (b) $SnO_2$/BiOBr/GCE, (c) dep Au/$SnO_2$/BiOBr/GCE, (d) capture DNA/dep Au/$SnO_2$/BiOBr/GCE, (e) MCH/capture DNA/dep Au/$SnO_2$/BiOBr/GCE, and (f) output DNA−$SiO_2$/MCH/capture DNA/dep Au/$SnO_2$/BiOBr/GCE.

$SnO_2$/BiOBr (2.5 mg/mL) composite was coated on the bare GCE surface and dried to gain a uniform film. Afterward, by immersing the modified electrode in 1% $HAuCl_4$ solution for 10 s at −0.2 V, the Au NP layer was electrodeposited onto the surface of the modified electrode (dep Au). Subsequently, the resultant electrode was incubated with 15 μL of capture DNA (2.5 μM) overnight at 4 °C to immobilize the capture DNA via Au−S bonds. Thereafter, 10 μL of 1 mM 6-mercaptohexanol (MCH) was incubated on the surface of the resultant electrode at room temperature for 0.5 h for blocking nonspecific binding sites. The sensing interface was constructed by such a process. The needless absorbed species were eliminated after each modification by carefully rinsing with ultrapure water. The specific construction procedure of this PEC biosensor was depicted in Scheme 1A.



https://doi.org/10.1021/acs.analchem.1c02745
Anal. Chem. 2021, 93, 12995−13000

## RESULTS AND DISCUSSION

**Characterization of the Prepared Materials.** The microstructures and morphologies of the synthesized materials were characterized by scanning electron microscopy (SEM). It can be seen that $SnO_2$ was in the form of nanoparticles with a size of about 30 nm (Figure 1A) and BiOBr illustrated a thin irregular flake structure with a smooth surface (Figure 1B). It could be observed that $SiO_2$ nanoparticles had a spherical structure with a size of about 40 nm (Figure 1C). These results suggested that the preparation of the above materials was successful. Figure 1D showed that $SnO_2$ nanoparticles were anchored on the surface of BiOBr nanosheets. Meanwhile, the SEM mapping images (Figure 1E) of Sn, O, Bi, and Br elements also confirmed the successful synthesis of the $SnO_2$/BiOBr composite. Besides, transmission electron microscopy (TEM) and X-ray diffraction (XRD) were conducted to further analyze the $SnO_2$/BiOBr composite (see the Supporting Information). As depicted in Figure 2A, the photoluminescence (PL) intensity of the $SnO_2$/BiOBr composite was weaker than that of pure $SnO_2$, demonstrating that the $SnO_2$/BiOBr complex owned a more efficient separation of the electron−hole pairs than that of pristine $SnO_2$.[24,30] Figure 2B illustrated that the $SnO_2$/BiOBr composite had significantly enhanced light absorption in the entire UV−vis range compared with the pristine $SnO_2$ and BiOBr.

**Electrochemical Characterization of Electrode Assembly.** Cyclic voltammetry (CV) and electrochemical impedance spectroscopy (EIS) measurements were conducted to evaluate the stepwise modification of this PEC biosensor. Figure 3 showed that compared with the bare GCE, the redox peak current (Figure 3A, curve b) and the charge-transfer resistance ($R_{et}$) (Figure 3B, curve b) both showed an obvious increase after modifying with the photoactive material $SnO_2$/BiOBr composite, which could be ascribed to the poor conductivity of uniform $SnO_2$/BiOBr film that could impede the transfer of electron. Subsequently, when the electrode surface was modified with the Au NP layer, an enhanced peak current (Figure 3A, curve c) and a decreased $R_{et}$ (Figure 3B, curve c) were observed on account of the fact that Au NPs embrace outstanding conductivity. After the capture DNA, MCH, and output DNA−$SiO_2$ were successively incubated onto the surface of the modified electrode, the peak currents (Figure 3A, curve d−f) illustrated a continuous reduction resulting from the increased electrostatic repulsion, poor conductivity, and steric hindrance, respectively, while the changing trend of impedance (Figure 3B, curve d−f) was opposite to that of CV. All the results illustrated that the stepwise construction of the biosensor was successful.

**PEC Characterization of Electrode Assembly.** PEC characterization was conducted to further verify the construction process of the biosensor. In Figure 4, the photocurrent intensity (curve a) was nearly zero for bare GCE, while the PEC response (curve b) displayed a significant increase when the $SnO_2$/BiOBr composite was coated onto the electrode. After dep Au, an enhanced PEC response was obtained (curve c) since the conductivity of Au NPs is brilliant and the plasmonic effect of Au NPs can promote charge separation. When capture DNA and MCH were incubated onto the surface of the resultant electrode continuously, the photocurrent (curves d and e) revealed successive reduction owing to the poor conductivity of DNA and MCH. With output DNA−$SiO_2$ anchored onto the modified electrode, the photocurrent decreased obviously on account of the steric-hindrance effect of $SiO_2$. These characterization data indicated that this biosensor was successfully fabricated.

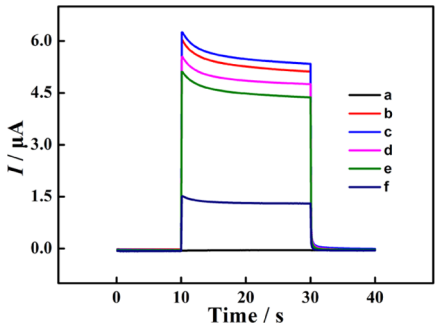


**Figure 4.** PEC characterization of (a) bare GCE, (b) $SnO_2$/BiOBr/GCE, (c) dep Au/$SnO_2$/BiOBr/GCE, (d) capture DNA/dep Au/$SnO_2$/BiOBr/GCE, (e) MCH/capture DNA/dep Au/$SnO_2$/BiOBr/GCE, and (f) output DNA−$SiO_2$/MCH/capture DNA/dep Au/$SnO_2$/BiOBr/GCE.

**Analysis Performance Test.** To assess the detection performance of this developed biosensor, the photocurrent signals subject to target DNA with a series of different concentrations were measured. As revealed in Figure 5A, in the range of 0.5 fM to 5 nM, with the increase in target concentration, the photocurrent response linearly diminished. The corresponding linear equation was demonstrated in Figure 5B, which was $I = -0.1971 \lg c + 1.050$ ($R^2 = 0.9964$), where $I$, $c$, and $R^2$ were the photocurrent intensity, the concentration of target DNA, and the correlation coefficient, respectively. Moreover, the limit of detection was calculated as 0.18 fM (S/N = 3). Additionally, the analytic performance comparison was conducted between this elaborated PEC biosensor and other previous detection techniques for DNA detection. Apparently, Table 1 clearly illustrated that this constructed PEC assay owned a pretty lower detection limit and a much wider linear range.

**Specificity and Stability Test.** The specificity of the established biosensor was studied by monitoring the PEC responses toward target DNA (0.5 pM) and its interferents (50 pM) including the mixture sequences, single-base mismatch DNA 1 (smDNA 1), smDNA 2, and double-bases mismatch DNA (dmDNA). Figure 6A showed that the photocurrent response toward smDNA 1, smDNA 2, and dmDNA displayed a negligible change while an obvious quenching of the photocurrent intensity was obtained after introducing mixture sequences and target DNA, which indicated that the designed biosensor embraced desirable specificity. Furthermore, the stability of the developed biosensor was evaluated by monitoring the photocurrent signal with 0.5 pM target DNA under 10 consecutive light "off−on−off" cycles. Figure 6B revealed a negligible change in the photocurrent and 0.8% of the relative standard deviation (RSD), indicating that this designed strategy embraced exceptional stability.

**Preliminary Application Investigation.** The application potential of this developed biosensor was evaluated by the standard addition method. Different concentrations of target DNA spiked in healthy serum samples (50-fold diluted) were detected. As depicted in Table S2 (showed in the Supporting Information), with recovery ranging from 96.7 to 104.2% and


https://doi.org/10.1021/acs.analchem.1c02745
Anal. Chem. 2021, 93, 12995−13000

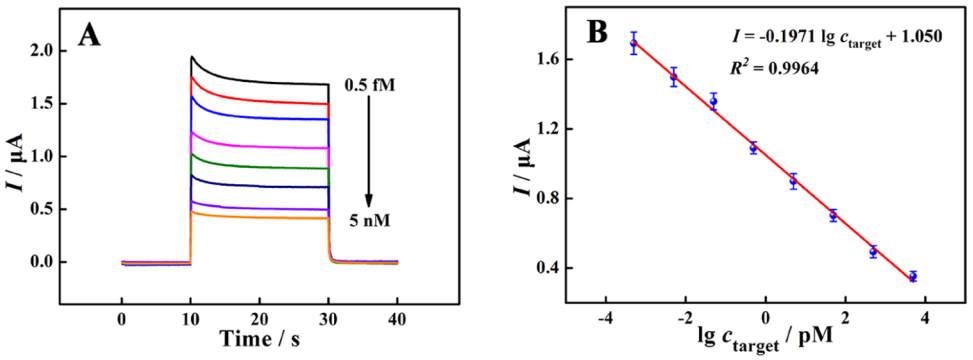


**Figure 5.** (A) PEC response of this biosensor corresponding to target DNA with concentrations ranging from 0.5 fM to 5 nM (from top to bottom: 0.5 fM, 5 fM, 50 fM, 0.5 pM, 5 pM, 50 pM, 0.5 nM, 5 nM). (B) Response relationship of photocurrent and lg $c_{target}$.

**Table 1. Comparison of Other Reported Techniques with This Assay for the Determination of DNA**

| analytical method | detection limit | linear range | ref |
|---|---|---|---|
| electrochemiluminescence | 0.18 fM | 1 fM to 100 pM | 34 |
| electrochemistry | 8.74 fM | 20 fM to 5 nM | 35 |
| colorimetry | 14.6 pM | 25 pM to 5 nM | 36 |
| fluorescence | 0.1 fM | 0.5 fM to 1 pM | 37 |
| PEC | 0.5 nM | 1 nM to 10 $\mu$M | 38 |
| PEC | 0.64 fM | 2 fM to 50 nM | 39 |
| PEC | 0.18 fM | 0.5 fM to 5 nM | this work |

RSD varying between 2.9 and 4.8%, the fabricated PEC biosensor illustrated application potential in real samples.

## CONCLUSIONS

An elegant PEC strategy was designed for ultrasensitive DNA determination depending upon a p−n heterojunction $SnO_2$/BiOBr with desirable photoelectric conversion efficiency as the photoactive matrix and $SiO_2$ as the effective signal quencher. Impressively, the formation of $SnO_2$/BiOBr p−n heterojunction not only depressed the electron−hole recombination but also expanded the light absorption in the UV−vis region, thereby further improving the photoelectric conversion efficiency of $SnO_2$. Notably, the photocurrent of the $SnO_2$/BiOBr heterojunction illustrated 6.4-fold and 12.1-fold increase over the pristine BiOBr and $SnO_2$, respectively, due to the formation of a large built-in electric field. Besides, $SiO_2$ as the signal quencher could significantly quench the photocurrent intensity of the $SnO_2$/BiOBr heterojunction. The detection sensitivity of the PEC biosensor was improved remarkably through coupling Nt·BstNBI enzyme-assisted target cyclic procedure with the effective quenching effect of $SiO_2$. Consequently, the established PEC strategy opens a new avenue for constructing heterojunction with extraordinary photoactive performance and monitoring various kinds of biomarkers.

## ASSOCIATED CONTENT

### Supporting Information

The Supporting Information is available free of charge at https://pubs.acs.org/doi/10.1021/acs.analchem.1c02745.

Materials and reagents, sequences utilized in this work (Table S1), instruments, optimization of the volume of $H_2O_2$ (Figure S1), experimental conditions, characterization of Au NPs (Figure S2), characterization of $SnO_2$/BiOBr composite (Figure S3), synthesis of $SiO_2$−$NH_2$ NPs, comparison of PEC signals about different nanomaterials (Figure S4), characterization of hairpin DNA−$SiO_2$ conjugate (Figure S5), and investigation of application potential of this PEC biosensor (Table S2) (PDF)

## AUTHOR INFORMATION

### Corresponding Authors

**Yaqin Chai** − *Key Laboratory of Luminescence Analysis and Molecular Sensing (Southwest University), Ministry of Education, College of Chemistry and Chemical Engineering, Southwest University, Chongqing 400715, P. R. China;* orcid.org/0000-0003-4392-9592; Phone: +86-23-

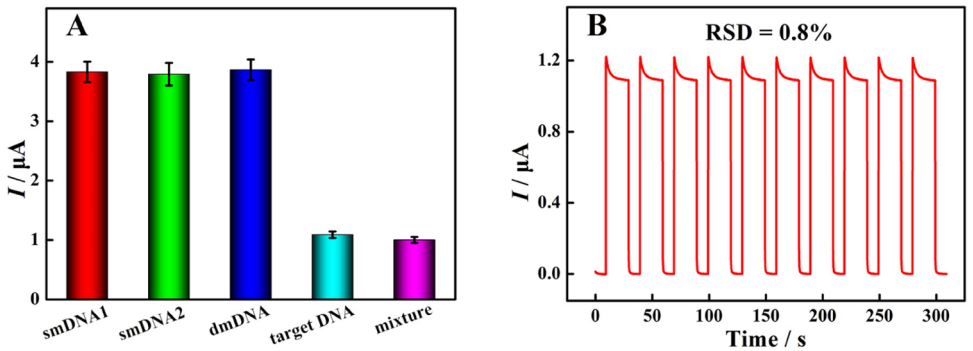


**Figure 6.** (A) Selectivity of the biosensor corresponding to different samples: smDNA 1, smDNA 2, dmDNA, the mixture, and target DNA. (B) Stability survey of the biosensor toward 0.5 pM target DNA.



https://doi.org/10.1021/acs.analchem.1c02745
Anal. Chem. 2021, 93, 12995−13000

68252277; Email: yqchai@swu.edu.cn; Fax: +86-23-68253172

**Ruo Yuan** − *Key Laboratory of Luminescence Analysis and Molecular Sensing (Southwest University), Ministry of Education, College of Chemistry and Chemical Engineering, Southwest University, Chongqing 400715, P. R. China;* orcid.org/0000-0003-3664-6236; Email: yuanruo@swu.edu.cn

### Authors

**Dan Long** − *Key Laboratory of Luminescence Analysis and Molecular Sensing (Southwest University), Ministry of Education, College of Chemistry and Chemical Engineering, Southwest University, Chongqing 400715, P. R. China*

**Yupeng Tu** − *Key Laboratory of Luminescence Analysis and Molecular Sensing (Southwest University), Ministry of Education, College of Chemistry and Chemical Engineering, Southwest University, Chongqing 400715, P. R. China*

Complete contact information is available at: https://pubs.acs.org/10.1021/acs.analchem.1c02745

### Notes

The authors declare no competing financial interest.

## ■ ACKNOWLEDGMENTS

This work was financially supported by the National Natural Science Foundation of China (21974108, 21775124, and 21675129) and the Fundamental Research Funds for the Central Universities (XDJK2020TY002), China.

## ■ REFERENCES

(1) Feng, J. H.; Dai, L.; Ren, X.; Ma, H. M.; Wang, X. Y.; Fan, D. W.; Wei, Q.; Wu, R. D. *Anal. Chem.* **2021**, *93*, 7125−7132.
(2) Zhao, C. Q.; Zhou, J.; Wu, K. W.; Ding, S. N.; Xu, J. J.; Chen, H. H. *Anal. Chem.* **2020**, *92*, 6886−6892.
(3) Li, P. P.; Cao, Y.; Mao, C. J.; Jin, B. K.; Zhu, J. J. *Anal. Chem.* **2019**, *91*, 1563−1570.
(4) Li, H. B.; Han, M.; Weng, X.; Zhang, Y. Y.; Li, J. *ACS Nano* **2021**, *15*, 1710−1717.
(5) Ge, L.; Hong, Q.; Li, H.; Liu, C. C.; Li, F. *Adv. Funct. Mater.* **2019**, *29*, No. 1904000.
(6) Wang, J.; Lv, W. X.; Wu, J. H.; Li, H. Y.; Li, F. *Anal. Chem.* **2019**, *91*, 13831−13837.
(7) Shu, J.; Tang, D. P. *Anal. Chem.* **2020**, *92*, 363−377.
(8) Hu, D. L.; Liang, H. F.; Wang, X. Y.; Luo, F.; Qiu, B.; Lin, Z. Y.; Wang, J. *Anal. Chem.* **2020**, *92*, 10114−10120.
(9) Wang, S. P.; Wang, F. F.; Fu, C. P.; Sun, Y. N.; Zhao, J. G.; Li, N.; Liu, Y. Q.; Ge, S. G.; Yu, J. H. *Anal. Chem.* **2020**, *92*, 7604−7611.
(10) Yu, S. Y.; Zhang, L.; Zhu, L. B.; Gao, Y.; Fan, G. C.; Han, D. M.; Chen, G. X.; Zhao, W. W. *Coord. Chem. Rev.* **2019**, *393*, 9−20.
(11) Tan, J. S.; Peng, B.; Tang, L.; Zeng, G. M.; Lu, Y.; Wang, J. J.; Ouyang, X. L.; Zhu, X.; Chen, X.; Feng, H. P. *Anal. Chem.* **2020**, *92*, 13073−13083.
(12) Fu, C. F.; Li, X. X.; Yang, J. L. *Chem. Sci.* **2021**, *12*, 2863−2869.
(13) Lin, Y.; Cai, H. Z.; Chen, H. Y.; Luo, H. *Appl. Surf. Sci.* **2021**, *544*, No. 148921.
(14) Lei, B.; Xu, D. D.; Wei, B.; Xie, T. F.; Xiao, C. Y.; Jin, W. L.; Xu, L. L. *ACS Appl. Mater. Interfaces* **2021**, *13*, 4785−4795.
(15) Li, K.; Zeng, X. Q.; Gao, S. M.; Ma, L.; Wang, Q. Y.; Xu, H.; Wang, Z. Y.; Huang, B. B.; Dai, Y.; Lu, J. *Nano Res.* **2016**, *9*, 1969−1982.
(16) Zhu, L. Y.; Li, H.; Xia, P. F.; Liu, Z. R.; Xiong, D. H. *ACS Appl. Mater. Interfaces* **2018**, *10*, 39679−39687.
(17) Han, F. J.; Song, Z. Q.; Nawaz, M. H.; Dai, M. J.; Han, D. F.; Han, L. P.; Fan, Y. Y.; Xu, J. N.; Han, D. X.; Niu, L. *Anal. Chem.* **2019**, *91*, 10657−10662.
(18) Chen, Y. L.; Zuo, X. J.; He, Y. Y.; Qian, F.; Zuo, S. N.; Zhang, Y. L.; Liang, L.; Chen, Z. Q.; Zhao, K.; Liu, Z. K.; Gou, J.; Liu, S. Z. *Adv. Sci.* **2021**, *8*, No. 2001466.
(19) Zhuang, J.; Mao, P.; Luan, Y. G.; Chen, N. L.; Cao, X. F.; Niu, G. S.; Jia, F. F.; Wang, F. Y.; Cao, S. K.; Wang, J. Z. *Adv. Funct. Mater.* **2021**, *31*, No. 2010385.
(20) Wei, F. C.; Wang, T. T.; Jiang, X. L.; Ai, Y.; Cui, A. Y.; Cui, J.; Fu, J. W.; Cheng, J. G.; Lei, L. C.; Hou, Y.; Liu, S. H. *Adv. Funct. Mater.* **2020**, *30*, No. 2002092.
(21) Wang, X.; Lv, J.; Zhang, L. X.; Wang, X. L.; Xue, C. Z.; Bian, G. Q.; Li, D. S.; Wang, Y.; Wu, T. *Nanoscale* **2020**, *12*, 772−784.
(22) Zhang, L.; Tong, R. B.; Shirsath, S. E.; Yang, Y. L.; Dong, G. H. *J. Mater. Chem. A* **2021**, *9*, 5000−5006.
(23) Wu, J. J.; Zhang, Y. F.; Zhou, J. S.; Wang, K. N.; Zheng, Y. Z.; Tao, X. *Appl. Catal., B* **2020**, *278*, No. 119301.
(24) Wu, H. Z.; Yuan, C. W.; Chen, R. M.; Wang, J. D.; Dong, F.; Li, J. Y.; Sun, Y. J. *ACS Appl. Mater. Interfaces* **2020**, *12*, 43741−43749.
(25) Zhang, S. C.; Si, H. N.; Fan, W. Q.; Shi, M. Y.; Li, M. H.; Xu, C. Z.; Zhang, Z.; Liao, Q. L.; Sattar, A.; Kang, Z.; Zhang, Y. *Angew. Chem., Int. Ed.* **2020**, *59*, 11573−11582.
(26) Tang, Q. Y.; Yang, M. J.; Yang, S. Y.; Xu, Y. H. *J. Hazard. Mater.* **2021**, *407*, No. 124798.
(27) Lv, X. C.; Yan, D. Y. S.; Lam, F. L. Y.; Ng, Y. H.; Yin, S. M.; An, A. K. *Chem. Eng. J.* **2020**, *401*, No. 126012.
(28) Wang, X. Y.; Xu, G. Z.; Tu, Y. Z.; Wu, D. S.; Li, A. M.; Xie, X. C. *Chem. Eng. J.* **2021**, *411*, No. 128456.
(29) Wang, Z. W.; Chen, M.; Huang, D. L.; Zeng, G. M.; Xu, P.; Zhou, C. Y.; Lai, C.; Wang, H.; Cheng, M.; Wang, W. J. *Chem. Eng. J.* **2019**, *374*, 1025−1045.
(30) Liu, H. J.; Du, C. W.; Li, M.; Zhang, S. S.; Bai, H. K.; Yang, L.; Zhang, S. Q. *ACS Appl. Mater. Interfaces* **2018**, *10*, 28686−28694.
(31) Long, D.; Li, M. J.; Wang, H. H.; Wang, H. J.; Chai, Y. Q.; Li, Z. H.; Yuan, R. *Anal. Chem.* **2020**, *92*, 14769−14774.
(32) Wang, H. H.; Li, M. J.; Zheng, Y. N.; Hu, T.; Chai, Y. Q.; Yuan, R. *Biosens. Bioelectron.* **2018**, *120*, 71−76.
(33) Xia, L. Y.; Li, M. J.; Wang, H. J.; Yuan, R.; Chai, Y. Q. *Anal. Chem.* **2020**, *92*, 14550−14557.
(34) Lv, H. Y.; Chen, A. Y.; Cheng, W. Q.; Kong, L. S.; Zhao, M.; Ding, S. J.; Ju, H. X.; Cheng, W. *Anal. Chem.* **2020**, *92*, 15624−15631.
(35) Jiang, J.; Wu, H. Y.; Su, Y.; Liang, Y.; Shu, B. W.; Zhang, C. S. *Anal. Chem.* **2020**, *92*, 7708−7716.
(36) Chen, W. W.; Zhang, X. B.; Li, J. J.; Chen, L. Z.; Wang, N. N.; Yu, S. Q.; Li, G. M.; Xiong, L. F.; Ju, H. X. *Anal. Chem.* **2020**, *92*, 2714−2721.
(37) Liu, S.; Yu, X. X.; Wang, J. L.; Liu, D. R.; Wang, L.; Liu, S. F. *Anal. Chem.* **2020**, *92*, 9764−9771.
(38) Li, X.; Lu, J. M.; Feng, L. Z.; Zhang, L. Z.; Gong, J. M. *Anal. Chem.* **2020**, *92*, 11476−11483.
(39) Deng, H. M.; Zhu, M. H.; Huang, L. J.; Chai, Y. Q.; Liu, X. R.; Yuan, R.; Yuan, Y. L. *Anal. Chem.* **2019**, *91*, 12468−12475.